The Astrophysical Journal, 809:31 (16pp), 2015 August 10 doi:10.1088/0004-637X/809/1/31
© 2015. The American Astronomical Society. All rights reserved.

INFERRED INITIAL ^{26}Al/^{27}Al RATIOS IN PRESOLAR STARDUST GRAINS FROM SUPERNOVAE ARE HIGHER THAN PREVIOUSLY ESTIMATED

Evan Groopman[1], Ernst Zinner[1], Sachiko Amari[1], Frank Gyngard[1], Peter Hoppe[2], Manavi Jadhav[3], Yangting Lin[4], Yuchen Xu[4], Kuljeet Marhas[5], and Larry R. Nittler[6]
[1] Laboratory for Space Sciences, Physics Department, Washington University, One Brookings Drive, Campus Box 1105, Saint Louis, MO 63130, USA; eegroopm@physics.wustl.edu
[2] Max Planck Institute for Chemistry, Particle Chemistry Department, P.O. Box 3060, D-55020 Mainz, Germany
[3] Department of the Geophysical Sciences, University of Chicago, Chicago, IL 60637, USA
[4] Key Laboratory of Earth and Planetary Physics, Institute of Geology and Geophysics, Chinese Academy of Sciences, Beijing, 100029, China
[5] Planetary Sciences Division, Physical Research Laboratory, Ahmedabad, Gujarat, 380009 India
[6] Department of Terrestrial Magnetism, Carnegie Institution of Washington, 5241 Broad Branch Road NW, Washington, DC 20015, USA
Received 2015 April 30; accepted 2015 July 4; published 2015 August 6

ABSTRACT

We performed an in-depth exploration of the Al–Mg system for presolar graphite, SiC, and Si_3N_4 grains found to contain large excesses of ^{26}Mg, indicative of the initial presence of live ^{26}Al. Ninety of the more than 450 presolar grains processed in this study contain well-correlated δ^{26}Mg/^{24}Mg and ^{27}Al/^{24}Mg ratios, derived from Nano-scale Secondary Ion Mass Spectrometer depth profiles, whose isochron-like regression lines yield inferred initial ^{26}Al/^{27}Al ratios that, on average, are ∼1.5–2 times larger than the ratios previously reported for the grains. The majority of presolar graphite and SiC grains are heavily affected by Al contamination, resulting in large negative δ^{26}Mg/^{24}Mg intercepts of the isochron lines. Al contamination is potentially due to etching of the grains' surfaces and subsequent capture of dissolved Al during the acid dissolution of their meteorite host rocks. From the isochron fits, the magnitude of Al contamination was quantified for each grain. The amount of Al contamination on each grain was found to be random and independent of grain size, following a uniform distribution with an upper bound at 59% contamination. The Al contamination causes conventional whole-grain estimates to underpredict the initial ^{26}Al/^{27}Al ratios. The presolar grains with the highest ^{26}Al/^{27}Al ratios are from Type II supernovae whose isochron-derived initial ^{26}Al/^{27}Al ratios greatly exceed those predicted in the He/C and He/N zones of SN models.

Key words: dust, extinction – meteorites, meteors, meteoroids – nuclear reactions, nucleosynthesis, abundances – supernovae: general

1. INTRODUCTION

Radioisotopes, i.e., unstable isotopes that decay into stable ones, have played an important role in astrophysics, cosmochemistry, and geochemistry (Diehl 2011). The initial presence of short- and long-lived radioisotopes has been detected through the presence of their daughter isotopes in presolar stardust grains and various Solar System (SS) objects, e.g., chondrules and Ca–Al-rich inclusions (CAIs). They have provided evidence for stellar nucleosynthesis and have served as chronometers for dating of cosmochemical, geological, archaeological, and biological objects.

Until the beginning of the 1950s the production site of the elements heavier than and including carbon was controversial, with the Big Bang (Alpher & Herman 1950) and stellar nucleosynthesis (Hoyle 1946, 1954) being two contending hypotheses. The observation of Tc, an element without any stable isotopes, in the atmosphere of red giant branch (RGB) stars (Merrill 1952) gave unambiguous evidence for stellar nucleosynthesis. Among the Tc isotopes, ^{98}Tc has the longest half-life ($\tau_{1/2} = 4.2 \times 10^6$ years). With such a lifetime, no Tc could have survived from the time of the Big Bang. As a consequence, Tc must have been produced by nuclear reactions (by neutron capture) within the stars. A few years later, stellar nucleosynthesis was put on a sound theoretical foundation by the work of Burbidge et al. (1957) and Cameron (1957).

Evidence for continued nucleosynthesis in the Galaxy and in individual stellar sites has been obtained in the form of gamma-rays resulting from the decay of radioisotopes (e.g., Diehl et al. 2014). The first isotope from which gamma-rays were discovered and the best studied isotope is ^{26}Al with a half-life of 7.2×10^5 years (Diehl et al. 1993, 2006, 2007). It shows a broad distribution in the plane of the Galaxy, with core-collapse supernovae (SNe) and massive stars being the most likely sources. Another radioactivity for which a diffuse distribution in the Galaxy was found is ^{60}Fe ($\tau_{1/2} = 2.6 \times 10^6$ years; Wang et al. 2007). In contrast, gamma-rays from several other radioisotopes were observed to be associated with individual SN events. The decay of ^{56}Ni ($\tau_{1/2} = 6.1$ days), ^{56}Co ($\tau_{1/2} = 77.2$ days), ^{57}Co ($\tau_{1/2} = 272$ days), and ^{44}Ti ($\tau_{1/2} = 60$ years) power the light curves of core-collapse SNe (Leibundgut et al. 2003). Gamma-rays from the decay of the first three of these isotopes have been discovered from SN1987A (Matz et al. 1988; Leising & Share 1990). Recently, the decay of ^{56}Co has been detected in SN2014J (Diehl et al. 2015). Gamma ray emission from the decay of ^{44}Ti has been found in the SN remnants Cassiopeia A (Vink et al. 2001; Renaud et al. 2006; Grefenstette et al. 2014) and SN1987A (Boggs et al. 2015). Additionally, the distribution of ^{44}Ti in the SN remnants and its discrepancy with that of Fe has been taken as evidence for an asymmetric SN explosion (Grefenstette et al. 2014; Boggs et al. 2015).

Radioisotopes have been extensively used for dating because the decay of a given radioactive nuclide provides a steady clock. The half-lives of the isotopes cover a large range, from ^{14}C ($\tau_{1/2} = 5700$ years) for the dating of recent events, to isotopes such as ^{235}U ($\tau_{1/2} = 7.0 \times 10^8$ years),

Table 1
Radioisotopes in Presolar Grains

Radioisotope	Daughter Isotope	Half-life	Presolar Grain Type	Stellar Source	Reference
^{49}V	^{49}Ti	330 days	SiC, Graphite	SNe	(1)
^{22}Na	^{22}Ne	2.6 years	Graphite	SNe	(2)
^{44}Ti	^{44}Ca	60 years	SiC, Graphite, Hibonite	SNe	(3)
^{32}Si	^{32}S	153 years	SiC	SNe, post-AGB stars	(4), (5)
^{41}Ca	^{41}K	1.02×10^5 years	SiC, Graphite, Hibonite	SNe, RGB, and AGB stars	(6)
^{99}Tc	^{99}Ru	2.11×10^5 years	SiC	AGB stars	(7)
^{26}Al	^{26}Mg	7.17×10^5 years	SiC, Graphite, Corundum, Spinel, Hibonite, Silicate	SNe, RGB, and AGB stars	(8)
^{93}Zr	^{93}Nb	1.61×10^6 years	SiC	AGB stars	(9)

References. (1) Hoppe & Besmehn (2002), (2) Amari (2009), (3) Nittler et al. (1996), (4) Pignatari et al. (2013), (5) Fujiya et al. (2013), (6) Amari et al. (1996), (7) Savina et al. (2004), (8) Zinner et al. (1991), (9) Kashiv et al. (2010).

^{238}U ($\tau_{1/2} = 4.47 \times 10^9$ years), and ^{87}Rb ($\tau_{1/2} = 4.88 \times 10^{10}$ years) for dating of events as old as the SS (e.g., McSween & Huss 2010). Whereas absolute ages can be obtained with long-lived isotopes such as the three listed here, relative ages can be obtained from the decay products of so-called short-lived isotopes, i.e., isotopes that do not exist anymore, if they have been "live" at some point in the past.

The discovery of ^{26}Mg excesses in refractory CAIs from the carbonaceous chondrite Allende has provided incontrovertible evidence for the initial presence of ^{26}Al in the early SS (Lee et al. 1976). Whereas the early Al–Mg studies were made by Thermal Ionization Mass Spectrometry, the ion microprobe (Secondary Ion Mass Spectrometry; SIMS) has added a tremendous amount of data and today thousands of such measurements have been reported on a wide variety of early SS objects (Davis & McKeegan 2014). Since most CAIs have the "canonical" ^{26}Al/^{27}Al ratio of $\sim 5.2 \times 10^{-5}$ (Jacobsen et al. 2008), the absolute age of CAIs obtained from U–Pb dating provides an anchor point for the determination of relative ages based on the Al–Mg system. After the discovery of ^{26}Al, evidence for the presence of a series of other short-lived isotopes in early SS materials has been found (Meyer & Zinner 2006; Huss et al. 2009). Whereas the abundances of some of these radioisotopes can be explained as being the steady-state abundances in the SS environment of the Galaxy, others, such as ^{26}Al, require a late injection into the Solar Nebula (Huss et al. 2009).

Presolar grains are condensates from the ejecta of late-age stars, including core-collapse SNe, RGB stars, asymptotic giant branch (AGB) stars, novae, and born-again AGB stars (post-AGB stars that experienced a very late thermal pulse; Herwig et al. 2011). Presolar grains that survived the formation of the SS became entrained in asteroids and comets early in SS history. The grains were preserved in primitive (minimally altered) meteorites and cometary dust, from which they are isolated and studied in the laboratory. Isotopically anomalous Ne and Xe noble gases (Reynolds & Turner 1964; Black & Pepin 1969) were traced through successive acid dissolution steps of the meteorite host rock, resulting in the discovery of three refractory, carbonaceous presolar minerals: nanodiamond (Lewis et al. 1987), SiC (Bernatowicz et al. 1987; Tang & Anders 1988), and graphite (Amari et al. 1990). Other presolar grain phases were subsequently discovered through alternative chemical separations, in situ analyses of meteorite thin sections, and transmission electron microscopy (TEM); these include silicate (Messenger et al. 2003), hibonite ($CaAl_{12}O_{19}$; Choi et al. 1999), corundum (Al_2O_3; Hutcheon et al. 1994; Nittler et al. 1994), spinel ($MgAl_2O_4$; Nittler et al. 1994), silicon nitride (Si_3N_4; Nittler et al. 1995), and carbide subgrains within presolar SiC and graphite grains (Bernatowicz et al. 1991).

If one neglects the rather indirect evidence for ^{22}Na ($\tau_{1/2} = 2.6$ years) from the Ne component Ne–E(L) in presolar graphite grains (Amari 2009), the first direct evidence for the initial presence of a radioisotope in presolar grains was obtained for ^{26}Al in SiC in the form of large ^{26}Mg excesses (Zinner et al. 1991). Since then evidence for ^{26}Al was found in presolar graphite (Hoppe et al. 1995; Jadhav et al. 2013; Amari et al. 2014), corundum (Hutcheon et al. 1994; Nittler et al. 1994, 1997), hibonite (Choi et al. 1999; Nittler et al. 2008), spinel (Zinner et al. 2005), and silicate (Nguyen & Zinner 2004) grains. In SiC, graphite, corundum, and hibonite, Al/Mg ratios can be very high, so Mg sometimes consists mostly of radiogenic ^{26}Mg (^{26}Mg*). Because the Al/Mg ratio in spinel is low and ^{26}Mg is affected by other nucleosynthetic contributions, the identification of initial ^{26}Al in this mineral is more tenuous. In addition to ^{26}Al, several other short-lived radioisotopes have been identified in presolar grains based on excesses in their daughter isotopes. Table 1 gives a list of these isotopes, their daughter products, half-lives, the presolar grain types in which they were first found, and their stellar sources.

SIMS measurements over time yield depth profiles of the analyzed isotopes and isotope ratios. Zinner & Jadhav (2013) constructed isochron-like correlation plots for the Al–Mg, Ca–K, and Ti–Ca systems from SIMS depth profiles of presolar graphite grains from the Orgueil (CI1) carbonaceous chondrite. Many of these isochrons show near-perfect correlations among[7] δ^{26}Mg/^{24}Mg and ^{27}Al/^{24}Mg, δ^{41}K/^{39}K and ^{40}Ca/^{39}K,

[7] $\delta^{26}\mathrm{Mg}/^{24}\mathrm{Mg} = 1000 \times \left(\frac{(^{26}\mathrm{Mg}/^{24}\mathrm{Mg})_{\mathrm{sample}}}{(^{26}\mathrm{Mg}/^{24}\mathrm{Mg})_{\mathrm{standard}}} - 1 \right)$ in ‰.

Table 2
Meteorite Parent Bodies and Size Ranges For Presolar SiC and Graphite Grains Analyzed in This Study

Meteorite	Size/Density Fraction	Grain Type	Separation Size Range (μm)	Mean Size (μm)	Number of Grains	Reference
Indarch	IH6	SiC	0.25–0.45	⋯	12	(1)
Murchison	KJB	SiC	0.3–0.7	⋯	7	(2)
Murchison	KJE	SiC	0.5–0.8	⋯	13	(3)
Murchison	LS	SiC	2–10	3.7	4	(4), (5)
Murchison	LU	SiC	>10	11.6	4	(4), (5)
Qingzhen	QZR4	SiC	0.4–0.8	0.6	5	(6), (7)
Qingzhen	QZR5	SiC	0.8–2	1.4	3	(6), (7)
Murchison	KJE	Si_3N_4	0.5–0.8	⋯	1	(3)
Qingzhen	QZR4	Si_3N_4	0.8–2	⋯	2	(6), (7)
Murchison	KFA1	LD Graphite	>1	3.3 (4 grains)	7	(8), (9)
Orgueil	OR1d	LD Graphite	>1	4.4	32	(10), (11)
Total	⋯	⋯	⋯	⋯	90	⋯

Note. Only grains with well-correlated $\delta^{26}Mg/^{24}Mg$ and $^{27}Al/^{24}Mg$ are listed. Mean size corresponds only to grains in this study. (⋯) indicates that no size information is available.
References. (1) Zinner et al. (2007), (2) Hoppe et al. (2010), (3) Xu et al. (2015), (4) Zinner & Jadhav, unpublished, (5) Amari et al. (1994), (6) Lin et al. (2002), (7) Lin et al. (2010), (8) Amari et al. (2014), (9) Xu et al. (2012), (10) Groopman et al. (2012), (11) Jadhav et al. (2013).

and $\delta^{44}Ca/^{40}Ca$ and $^{48}Ti/^{40}Ca$, indicating the retention of radiogenic ^{26}Mg, ^{41}K, and ^{44}Ca from the decays of ^{26}Al, ^{41}Ca, and ^{44}Ti, respectively. As Zinner & Jadhav (2013) state, these are not true isochrons as they do not contain any temporal information; however, they resemble true isochrons and will be referred to as such here. In this paper we investigate in detail evidence for initial ^{26}Al in presolar graphite, SiC, and Si_3N_4 grains. Among all the radioisotopes identified to date in stardust, we restrict ourselves to ^{26}Al because by far most of the data on radioisotopes in presolar grains exist for this isotope. The Al–Mg system is additionally the simplest regarding contamination, as there is only one stable Al isotope; however, the same kind of analysis may be applied to the other isotopic systems, such as Ca–K and Ti–Ca, with numerous caveats (see Section 3.5). Furthermore, large Al/Mg ratios in many grains result in enormous ^{26}Mg excesses and avoid any problems with the positive identification of ^{26}Al. Inferred initial $^{26}Al/^{27}Al$ ratios in presolar grains are typically regarded as lower limits (e.g., Hoppe et al. 1995; Jadhav et al. 2013) due to uncertainties associated with contamination. We aim to quantify the amount of contamination present to further constrain inferred initial $^{26}Al/^{27}Al$ ratios from presolar grains.

2. SAMPLES AND EXPERIMENTAL METHODS

Isochrons reported in this paper were derived from more than 450 depth profiles of samples whose data were published in previous studies, including presolar graphite grains from the Orgueil (CI1; Jadhav et al. 2006; Groopman et al. 2012; Jadhav et al. 2013; Zinner & Jadhav 2013) and Murchison (CM2; Xu et al. 2012; Amari et al. 2014) carbonaceous chondrites, and SiC and Si_3N_4 from the Murchison (CM2; Hoppe et al. 2010; Xu et al. 2015) carbonaceous chondrite, and SiC and Si_3N_4 from the Indarch (EH4; Zinner et al. 2007) and Qingzhen (EH3; Lin et al. 2010) enstatite chondrites. The list of grains in this study, and the ranges of presolar grain sizes from each meteorite are given in Table 2. Each presolar grain from these studies was individually measured with the Nanoscale Secondary Ion Mass Spectrometer (NanoSIMS) 50 at Washington University in St. Louis, USA, the Max Planck Institute for Chemistry in Mainz, Germany, or the NanoSIMS 50(L) at the Carnegie Institution of Washington, DC, USA. For each grain, depth profiles were generated by rastering a primary ion beam across the grain's surface. The negative secondary ions $^{12,13}C^-$, $^{16,18}O^-$, $^{26,27}CN^-$, and $^{28,29,30}Si^-$ were first measured using a Cs^+ primary beam, after which an O^- primary beam was used to measure the positive secondary ions $^{24,25,26}Mg^+$, $^{27}Al^+$, and either $^{12}C^+$, $^{28}Si^+$, or $^{40}Ca^+$. Each depth profile was limited to several minutes measurement time to preserve material for subsequent measurements of different isotopic systems and for future coordinated TEM analyses. To test the effects of Al and Mg contamination in presolar graphite and SiC grains, where Al is only a minor element and Mg is a trace element, several presolar hibonite (Nittler et al. 2008) grains, whose major elements include Al, were also analyzed in this study (see Section 3.3).

Following Zinner & Jadhav (2013), isochrons were generated by dividing NanoSIMS depth profiles (e.g., Figure 1(a)) into 5-cycle bins, with the bin averages of $\delta^{26}Mg/^{24}Mg$ and $^{27}Al/^{24}Mg$ calculated and plotted on an isochron plot (Figures 1(b), 2). Error bars indicate the standard error of the mean $\delta^{26}Mg/^{24}Mg$ and $^{27}Al/^{24}Mg$ values in each bin. Each isochron line was fitted with Orthogonal Distance Regression (ODR), a total least-squares regression technique that includes both x- and y-error weighting (Boggs & Rogers 1990). The majority of least-squares algorithms only weigh y-errors, if any, and so the choice of abscissa/ordinate axes otherwise affects the fit result since the errors in $\delta^{26}Mg/^{24}Mg$ and $^{27}Al/^{24}Mg$ are correlated. As the name implies, ODR minimizes the orthogonal distance between each data point and the regression line, as opposed to minimizing the vertical distance. The isochrons display the correlation between the $\delta^{26}Mg/^{24}Mg$ and $^{27}Al/^{24}Mg$ ratios, whose slopes are related to the initial $^{26}Al/^{27}Al$ ratios by a factor of 1.393×10^{-4} (see Zinner & Jadhav 2013), assuming that $(^{26}Mg_{intrinsic}/^{24}Mg)_{sample} \sim (^{26}Mg/^{24}Mg)_{standard}$, where $^{26}Mg_{intrinsic}$ refers to the non-radiogenic ^{26}Mg present in the sample. This assumption was used throughout the paper when determining the presence of Al contamination (see Section 3.2). If Al contamination is minimal and the isochrons

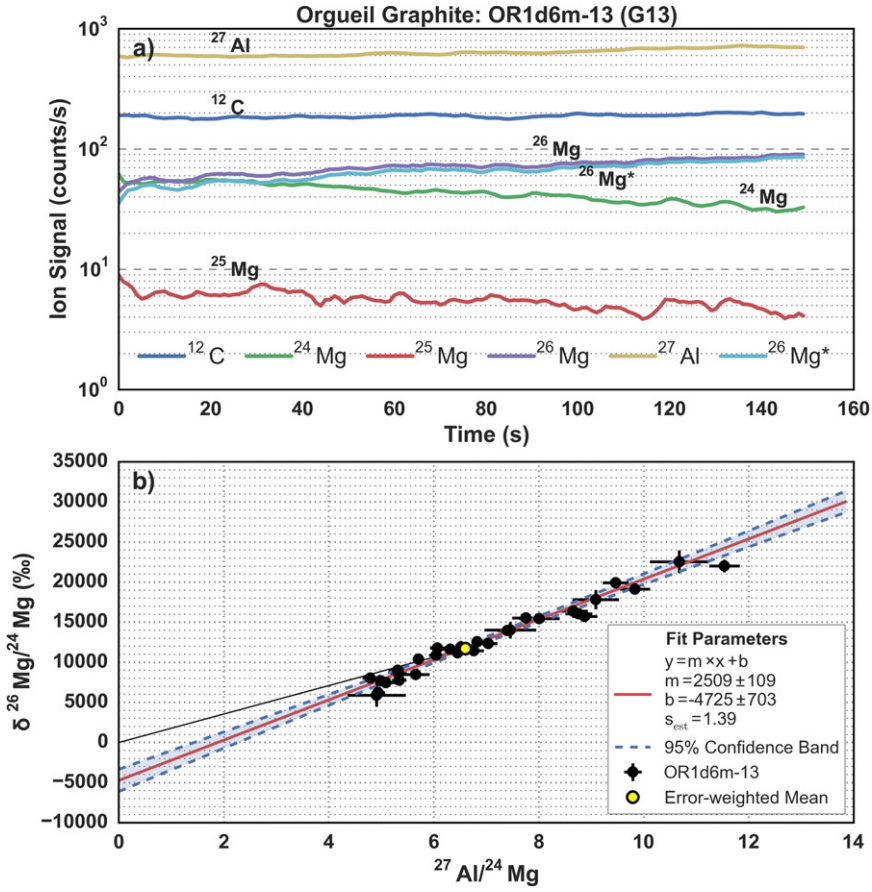

Figure 1. (a) Depth profile of LD presolar graphite grain OR1d6m-13 (G13; Groopman et al. 2012). This depth profile illustrates the significant difference in relative sensitivity between $^{12}C^+$ and $^{27}Al^+$ as measured by SIMS from a graphite matrix. Radiogenic ^{26}Mg ($^{26}Mg^*$) is the dominant component of the ^{26}Mg signal. Profiles are smoothed for visual clarity. (b) Al–Mg isochron with 95% confidence interval on the fit shown. Errors on fit parameters m and b are 1σ. The isochron slope of 2509 ± 109 corresponds to an initial $^{26}Al/^{27}Al$ ratio of $3.59 \times 10^{-1} \pm 1.52 \times 10^{-2}$, compared to the conventional whole-grain estimate of 2.31×10^{-1}. The $\delta^{26}Mg/^{24}Mg$ intercept of $-4725\% \pm 703‰$ indicates that approximately 29% of the measured Al is contamination. Error bars are the standard error of the mean ($\sigma_{\bar{x}}$) composition of each depth profile bin. s_{est} is the standard error of the estimate, equivalent to the square root of the residual variance, which describes the quantity of variation unexplained by the linear regression. Nearly all of the variation is described by the error bars on the data. The mean of the $\delta^{26}Mg/^{24}Mg$ and $^{26}Al/^{27}Al$ values is weighted by the inverse of the error on each point ($1/\sigma_{\bar{x}}$). The slope of the mean line is smaller than the isochron slope.

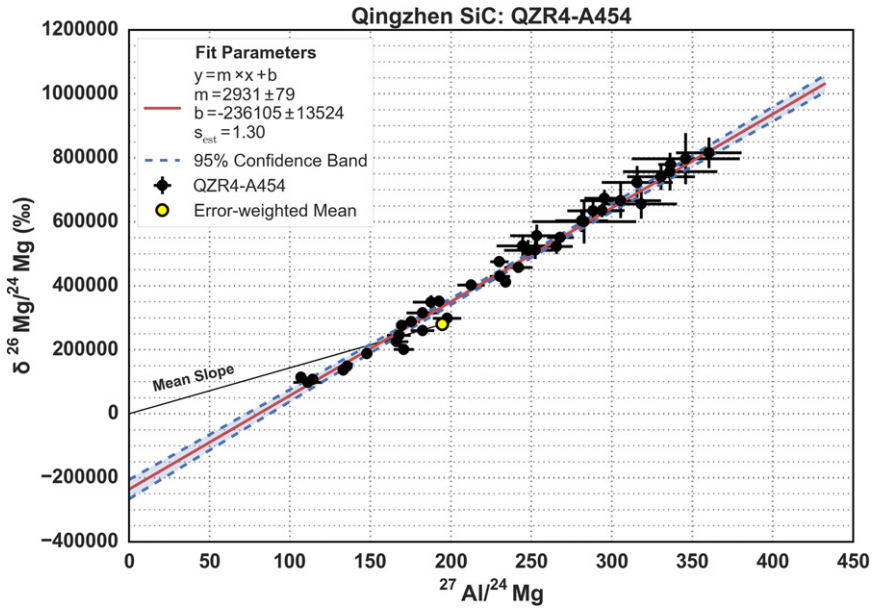

Figure 2. Isochron from Qingzhen SiC X grain QZR4-A454 (Lin et al. 2010). SiC grains have smaller relative $^{24}Mg^+$ ion signals, making error bars larger. The slope of 2931 ± 79 is equivalent to an initial $^{26}Al/^{27}Al$ ratio of $4.08 \times 10^{-1} \pm 1.11 \times 10^{-2}$, higher than the conventional whole-grain estimate of 2.48×10^{-1}. The negative intercept of $-236105\% \pm 13524‰$ can be explained by approximately 41% Al contamination.

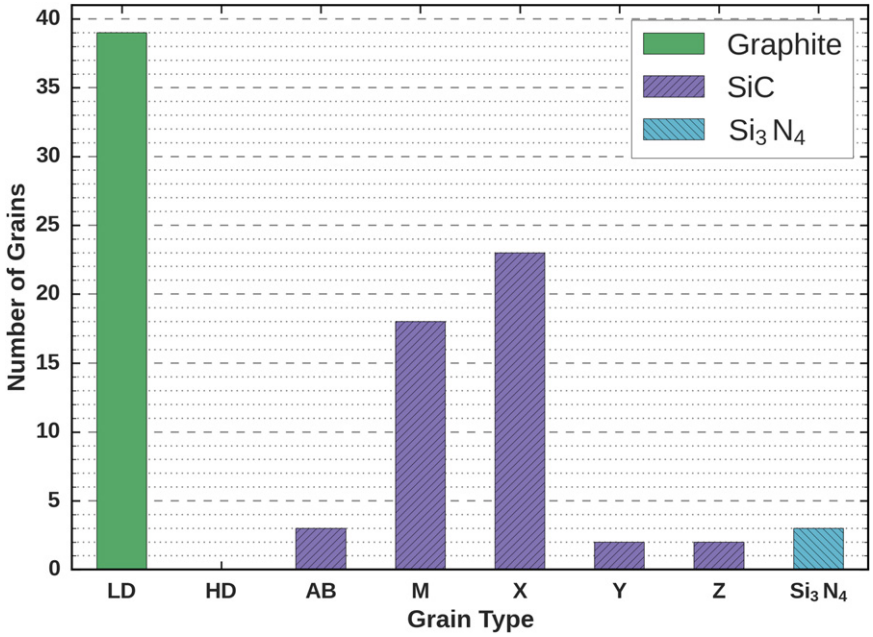

Figure 3. Breakdown of presolar grain type for the 90 grains with well-correlated $\delta^{26}Mg/^{24}Mg$ and $^{27}Al/^{24}Mg$ ratios in this study. Isochron fits were derived for 39 LD presolar graphite grains; 48 SiC grains: 3 AB, 18 Mainstream (M), 23 X, 2 Y, and 2 Z grains; and 3 Si_3N_4 grains.

have large positive $\delta^{26}Mg/^{24}Mg$ intercepts, the relationship between the isochron slope and the initial $^{26}Al/^{27}Al$ ratio is slightly more complicated, although easily derived from a $^{26}Mg/^{24}Mg$ versus $^{26}Al/^{27}Al$ correlation plot.

The conventional method for calculating the initial $^{26}Al/^{27}Al$ ratio of a presolar grain involves estimating the radiogenic component of the ^{26}Mg ion signal and taking its ratio relative to the ^{27}Al ion signal by assuming that the intrinsic $^{26}Mg/^{24}Mg$ ratio of the sample is that of the standard:

$$^{26}Mg^{*\dagger} = {}^{26}Mg^{\dagger}_{counts} - {}^{24}Mg^{\dagger}_{counts} \times \left(\frac{^{26}Mg}{^{24}Mg}\right)_{standard} \quad (1)$$

$$\frac{^{26}Al^{\dagger}}{^{27}Al^{\dagger}} = \frac{^{26}Mg^{*\dagger}}{^{27}Al^{\dagger}} \quad (2)$$

where † indicates ionic, not atomic abundances. This is effectively the same as forcing a line through both the origin and the mean composition of the grain on a $\delta^{26}Mg/^{24}Mg$ and $^{27}Al/^{24}Mg$ correlation plot. This was the method used to derive $^{26}Al/^{27}Al$ ratios given in the Presolar Grain Database (PGD; Hynes & Gyngard 2009). Any model estimate for the initial $^{26}Mg/^{24}Mg$ ratio of the grain could be used, however the terrestrial ratio is conventional. Importantly, the ionization efficiency of each element measured in a SIMS instrument depends upon the element's first ionization potential and the properties of the sample matrix. For instance, in Figure 1(a), the $^{12}C^+$ ion signal is smaller than the $^{27}Al^+$ signal, despite the presolar graphite grain being composed overwhelmingly of C, and Al being only a minor element. Positive C ions are generated much less readily than positive Al ions, with the precise ratio modulated by the sample matrix, i.e., graphite. The $^{26}Mg^{*\dagger}/^{27}Al^{\dagger}$ ratio must therefore be adjusted by a relative sensitivity factor, f, in order to recover each isotope's atomic abundance within the grain:

$$\frac{^{26}Al}{^{27}Al} = f \times \frac{^{26}Mg^{*\dagger}}{^{27}Al^{\dagger}}. \quad (3)$$

In order to calculate the relative sensitivity of the SIMS instrument to each ion species, a known stoichiometric standard must be used. Terrestrial (Burma) and meteoritic (from the Murray CM2 chondrite) spinel were used to correct for the relative sensitivity between Al and Mg. For spinel, the atomic ratio of Al/Mg is 2 and the $^{27}Al/^{24}Mg$ ratio is $2/0.79 \approx 2.53$. In a NanoSIMS measurement, the atomic $^{27}Al/^{24}Mg$ ratio is related to the ionic ratio by the sensitivity factor:

$$\frac{^{27}Al}{^{24}Mg} = \frac{1}{f} \times \frac{^{27}Al^{\dagger}}{^{24}Mg^{\dagger}} \quad (4)$$

$$f = \frac{0.79}{2} \times \frac{^{27}Al^{\dagger}}{^{24}Mg^{\dagger}} \quad (5)$$

where $^{27}Al^{\dagger}/^{24}Mg^{\dagger}$ is the ratio measured in a standard. The relative sensitivity, f, may then be substituted into Equation (3) to infer a presolar grain's initial $^{26}Al/^{27}Al$ ratio. Al/Mg sensitivity factors are typically between 1.5 and 2 (Zinner & Jadhav 2013). This approach cannot correct for matrix differences between the spinel standard and the SiC and graphite samples, however, there are currently no good matrix-matched standards for these presolar minerals and elements that are homogeneous at NanoSIMS-scale spatial resolutions. Isochron fits for grains with well-correlated $^{27}Al/^{24}Mg$ and $\delta^{26}Mg/^{24}Mg$ ratios can provide more information than the conventional whole-grain estimates as they include both initial $^{26}Al/^{27}Al$ ratios (slope) and intrinsic $^{26}Mg/^{24}Mg$ ratios (intercept). In this study the latter is assumed to be approximately that of the standard. For the correlation plots, the relative sensitivity factor is accounted for in the $^{27}Al/^{24}Mg$ axis values.

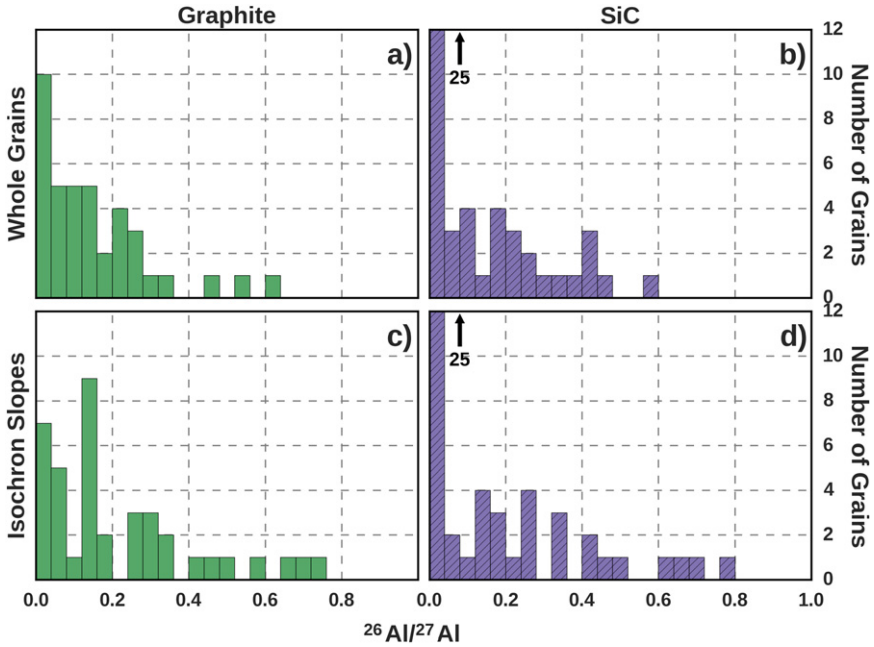

Figure 4. Comparison of inferred initial $^{26}Al/^{27}Al$ ratios from whole-grain measurements and from isochron slopes for presolar graphite and SiC grains.

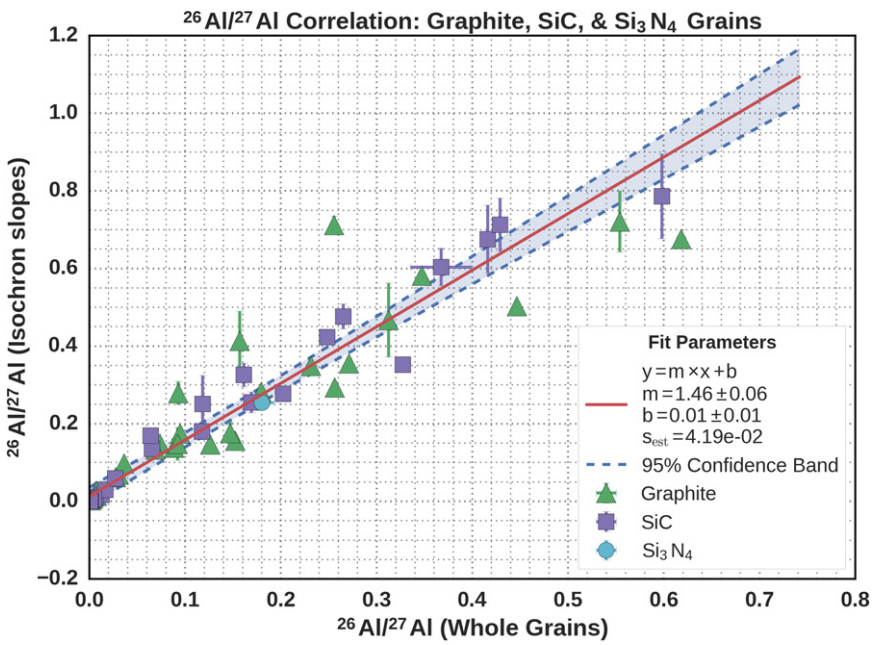

Figure 5. Inferred initial $^{26}Al/^{27}Al$ ratios derived from isochron slopes are approximately 50% higher than those estimated from whole-grain measurements for grains with negative $\delta^{26}Mg/^{24}Mg$ intercepts. Shown: ODR fit and 95% confidence interval on the fit to correlation data. Fit parameters: slope (m) = 1.46 ± 0.06, intercept (b) = 0.01 ± 0.01. Linear regressions to only presolar SiC or graphite grain populations yielded slopes of 1.5 and 1.4, respectively. The slope does not depend upon the relative $^{27}Al/^{24}Mg$ sensitivity factor as this factor is incorporated into both whole-grain and isochron slope estimates.

3. RESULTS AND DISCUSSION

3.1. Mg–Al Isochrons

Ninety of the more than 450 presolar grain depth profiles processed in this study exhibited well-correlated $\delta^{26}Mg/^{24}Mg$ and $^{27}Al/^{24}Mg$ ratios with minimal scatter around a linear best-fit line (e.g., Figures 1(b) and 2). Figure 3 shows the breakdown of these 90 presolar grains by type, including 39 low-density (LD; $1.6 < \rho < 2.05\,g\,cm^{-3}$) graphite grains; 48 SiC grains: 3 AB, 18 Mainstream (M), 23 X, 2 Y, and 2 Z grains; and 3 Si_3N_4 grains. No high-density (HD; $\rho > 2.05\,g\,cm^{-3}$) graphite grains with well-correlated $\delta^{26}Mg/^{24}Mg$ and $^{27}Al/^{24}Mg$ ratios were found. A SN origin has been posited for SiC X grains, for Si_3N_4 grains, and for LD graphite grains, which exhibit a wide range of $^{12}C/^{13}C$ ratios and excesses in ^{15}N, ^{18}O (graphite only), and ^{28}Si (Hoppe et al. 1995; Jadhav et al. 2006, 2013; Zinner et al. 2014). AB grains, with $^{12}C/^{13}C$ ratios <10 are thought to form in J-stars or in born-again AGB stars (Amari et al. 2001a; Fujiya et al. 2013). Mainstream grains have isotopic signatures

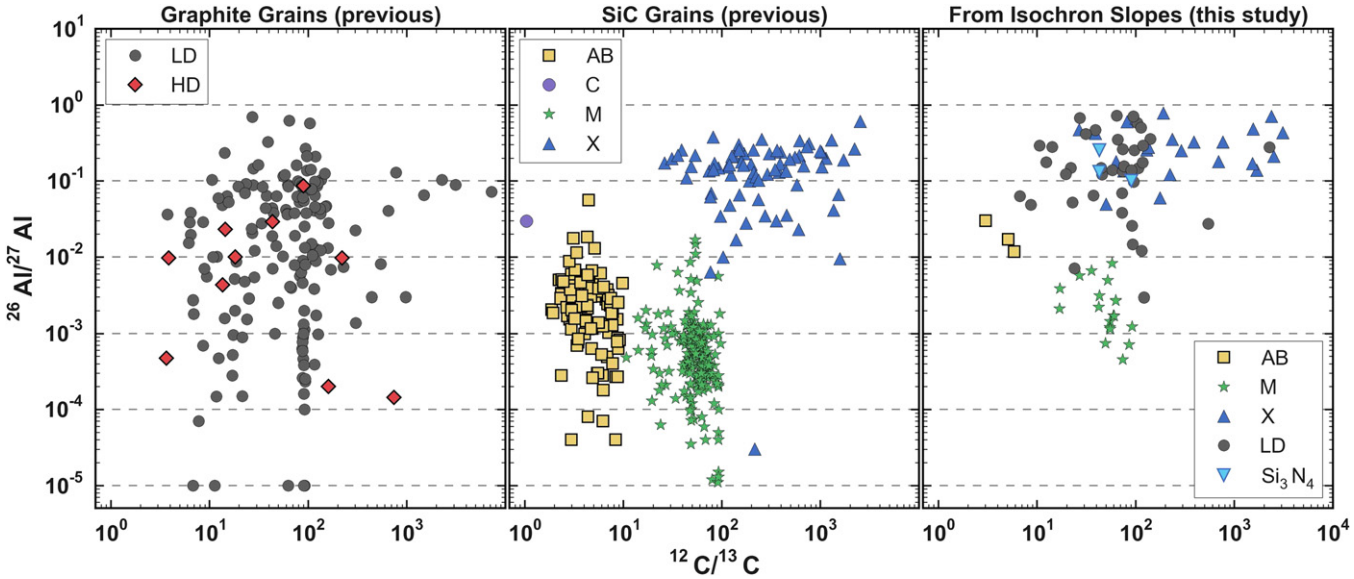

Figure 6. Ranges of $^{12}C/^{13}C$ and $^{26}Al/^{27}Al$ ratios in presolar graphite and SiC grains (PGD; Hynes & Gyngard 2009, p. 1198). $^{26}Al/^{27}Al$ ratios are compared to those inferred from isochron slopes in this study. SiC Y and Z grains are not included. The ratios shown in the third panel correspond only to grains with well-correlated $\delta^{26}Mg/^{24}Mg$ and $^{27}Al/^{24}Mg$ ratios.

consistent with an AGB star origin. AGB stars also produce ^{26}Al, though typically with lower $^{26}Al/^{27}Al$ ratios than SNe. Y and Z grains are inferred to form in the outflows of low-to-intermediate-mass AGB stars with low metallicities (Hoppe et al. 1997; Amari et al. 2001b).

The distributions of initial $^{26}Al/^{27}Al$ ratios are similar for presolar graphite and SiC grains for values derived from either isochron slopes or from conventional whole-grain measurements (Figure 4). The inferred initial $^{26}Al/^{27}Al$ ratios derived from isochron slopes are larger than those derived from whole-grain measurements by an average factor of 1.46 ± 0.06 (Figure 5). Linear regressions of the SiC and graphite grain populations separately yield factors of 1.52 ± 0.05 and 1.38 ± 0.12, respectively. For the majority of grains analyzed here, Al contamination appears to shift their isochrons rightward and their $\delta^{26}Mg/^{24}Mg$ intercepts to negative values, resulting in an underestimation of their true intrinsic $^{26}Al/^{27}Al$ ratios by a factor of ~1.5 on average when using conventional whole-grain methods (see next section).

These results only describe the sample of grains reported here with highly correlated $\delta^{26}Mg/^{24}Mg$ and $^{27}Al/^{24}Mg$ ratios. There exist numerous grains from previous studies with ^{26}Mg excesses and inferred $^{26}Al/^{27}Al$ ratios (Figure 6), but whose correlation plots show large amounts of scatter. These grains cannot be described by the methods detailed in this paper and additionally make it difficult to generalize these results to all presolar grains with ^{26}Mg excesses.

3.2. Al Contamination

The majority of grains analyzed in this study containing correlated $\delta^{26}Mg/^{24}Mg$ and $^{27}Al/^{24}Mg$ have isochrons that negatively intercept the $\delta^{26}Mg/^{24}Mg$ axis, most often with values less than minus 1000‰ (e.g., Figures 1(b) and 2). As these values would otherwise correspond to negative intrinsic $^{26}Mg/^{24}Mg$ ratios, which are nonsensical, instead they indicate that these measurements were affected by a constant fraction of Al contamination (see appendix of Zinner & Jadhav 2013),

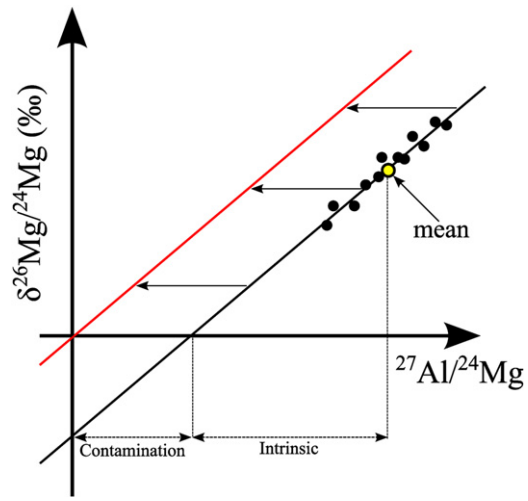

Figure 7. Schematic diagram illustrating how the degree of constant Al contamination was estimated for each isochron fit based on the fraction of the Al signal required to shift the isochron from its intercept on the $^{27}Al/^{24}Mg$ axis to an intercept through the origin. This shift was taken relative to the error-weighted mean $^{27}Al/^{24}Mg$ ratio. Addition of isotopically normal Mg moves the data points leftward down the isochron line, yielding larger inferred Al contamination due to lower mean $^{27}Al/^{24}Mg$ ratios.

which shifted the isochrons rightward and their $\delta^{26}Mg/^{24}Mg$ intercepts to more negative values. The data points for each correlation plot typically do not deviate drastically from the isochron fit, implying that the Al contamination did not change with sputtering depth. Zinner & Jadhav (2013) found no evidence for the loss of radiogenic $^{26}Mg^*$, which is corroborated by the examination of presolar hibonite grains (Section 3.3). While models of core-collapse Type II SNe (e.g., Rauscher et al. 2002) predict positive $\delta^{26}Mg/^{24}Mg$ values in their He/C and He/N zones, we may estimate a lower bound on the quantity of Al contamination in each measurement by solving for the (negative) horizontal shift required for the isochron to intercept the origin (Figure 7). The amount of Al

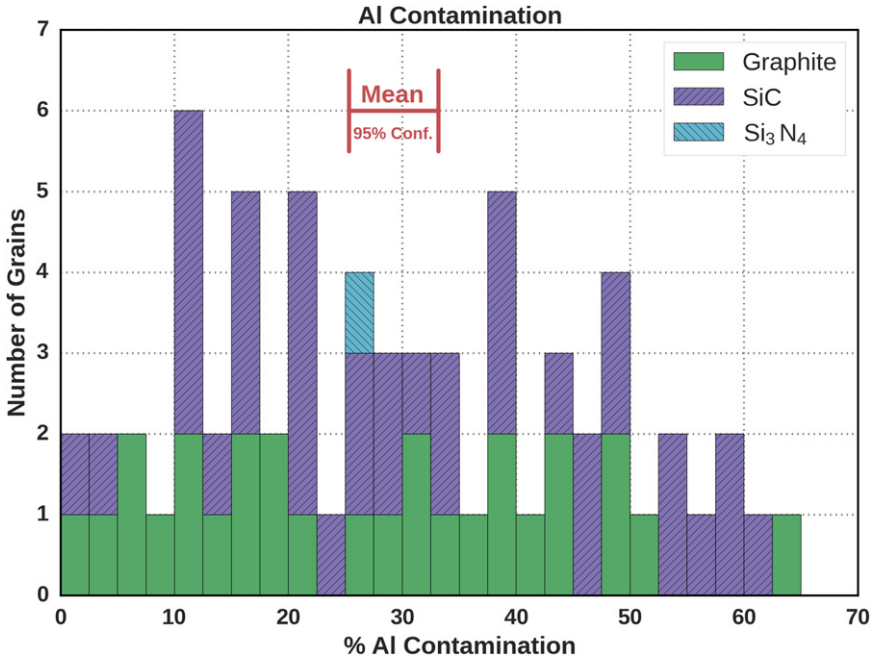

Figure 8. Estimated Al contamination (%) from isochrons with negative $\delta^{26}Mg/^{24}Mg$ intercepts. Histograms are stacked. The mean fractional Al contamination for the total distribution is 29% with a bootstrapped 95% confidence interval between 25% and 33%. There is no significant difference between graphite and SiC contamination distributions. The total distribution is best fitted by a sample drawn from a continuous uniform distribution with an upper bound at 59% (Figure 9).

contamination inferred from the isochrons ranges up to 63% of the total $^{27}Al^{+}$ signal in some grain measurements (Figure 8). Sixty-eight of the 90 grains have negative $\delta^{26}Mg/^{24}Mg$ intercepts, showing that a significant fraction of their Al signal is not intrinsic. For the grains with isochrons intercepting the origin or the positive $\delta^{26}Mg/^{24}Mg$ axis, no Al contamination estimate was made.

The distributions of fractional Al contamination are similar for both presolar graphite and SiC grains (Figure 8). The Kruskal–Wallis H-test, a non-parametric version of analysis of variance for samples that are not normally distributed, confirms the null hypothesis that the medians of the distributions are not significantly different with a nominal significance (p-value) of 0.37. A two-sample Kolmogorov–Smirnov (KS) test similarly shows that we cannot reject the null hypothesis that the SiC and graphite samples are drawn from the same distribution ($p = 0.78$). Since the individual contamination distributions are not significantly different, we combine them for the benefits of a larger sample size. Bootstrap resampling-with-replacement of the combined SiC and graphite contamination distribution yields a mean contamination value of 29% with a 95% confidence interval between 25% and 33%. The standard deviation of the binned data is 17% with a 95% confidence interval between 15% and 20%. The combined sample distribution has a skewness of 0.21, with a bootstrapped 95% confidence interval between −0.14 and 0.59, implying that the distribution is symmetric ($p = 0.45$; Bulmer 1979). We therefore tested whether the total Al contamination distribution was drawn from a continuous uniform distribution of contamination values, which would imply that there is no preference for a specific quantity of contamination, i.e., each grain's Al contamination is random and independent of other grains. We used a one-sided KS test to compare the sample distribution to uniform distributions with upper bounds varying between 0 and 1. We also examined the shape of the cumulative sample distribution (CSD) and compared it to that of a cumulative uniform distribution (Figure 9).

The one-sided KS test is a non-parametric test of equality between a sample and a continuous one-dimensional distribution with the null hypothesis that the sample is drawn from the distribution. Uniform distributions with lower bounds at 0 and upper bounds (cutoff) varying between 0 and 1 were compared to the sample distribution. For cutoff values between 47% and 70%, the null hypothesis may be accepted (Figure 9(a)), i.e., we cannot distinguish the presolar grain contamination distribution from a uniform distribution. Cutoff values outside of this range may be rejected with high significance.

For a uniform distribution with lower and upper bounds (0 and b) in the range [0, 1], the cumulative distribution increases linearly between 0 and b with a slope of $1/b$. The CSD is fitted by a slope 1.69 line (Figure 9(b)) which indicates that the sample distribution is drawn from a uniform distribution with a cutoff of 59%. The CSD is not biased in any direction about the linear fit, which implies that the linear fit is appropriate. The CSD does not readily match the cumulative distributions of other well-known distributions. While p-values do not indicate the probability of the null hypothesis being correct, the peak of the p-value distribution matches the cutoff value inferred from the linear regression of the cumulative distribution.

From these tests we conclude that the distribution of fractional Al contamination values is uniform up to ∼59%, implying that each grain's quantity of contamination is random and independent of any other grain. Figures 10(a)–(d) shows the lack of correlation between Al contamination and grain size, $^{27}Al/^{24}Mg$ ratio, $^{12}C/^{13}C$ ratio, $^{26}Al/^{27}Al$ ratio. Panels (e)–(f) show violin plots illustrating the distributions and kernel densities (envelopes) of Al contamination values for each subpopulation of presolar grains by type and meteorite host

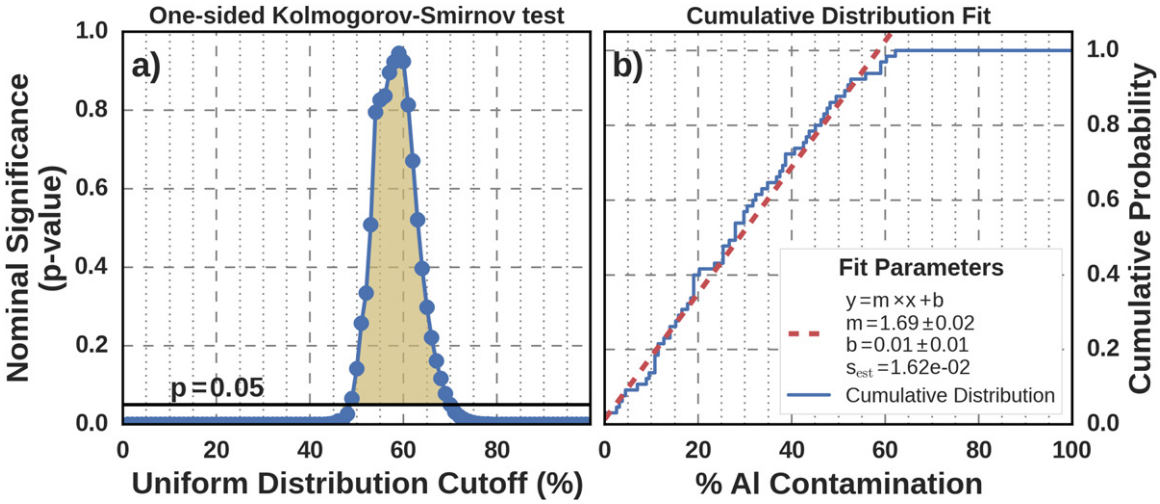

Figure 9. (a) Distribution of *p*-values for one-sided Kolmogorov–Smirnov tests between the total Al contamination distribution and continuous uniform distributions with varying upper cutoff values. For cutoff values within the range [47%, 70%] the null hypothesis that the distributions are equivalent may be accepted. (b) Linear regression to the normalized cumulative sample distribution (CSD) whose slope corresponds to a cutoff value of 59% for a uniform distribution.

rock. The subpopulations span similar ranges of Al contamination and are not sharply peaked near any value, implying that there is no correlation between Al contamination and presolar grain type or meteorite host rock. The uniform distribution up to 59% most likely reflects an upper bound on the quantity of Al contamination, however. The addition of isotopically normal Mg contamination, which was not accounted for here, has the effect of shifting correlation points down the isochron line toward lower $^{27}Al/^{24}Mg$ and $\delta^{26}Mg/^{24}Mg$ values. This reduces the mean $^{27}Al/^{24}Mg$ ratio for each grain, which results in higher inferred Al contamination, effectively stretching the contamination histogram to higher values.

The quantification of fractional Al contamination and therefore the inference of initial $^{26}Al/^{27}Al$ ratios from the isochron slopes relies on the assumption of constant Al contamination throughout each grain's depth profile. It must be emphasized that constant Al contamination through the depth profile does not imply constant Al contamination throughout the entire grain. Still, this assumption may appear unintuitive, especially given the structural differences between SiC and graphite grains. Each isochron reported here was fitted to a correlation plot with very little scatter about the isochron line. Retaining near-perfect correlation lines with non-constant Al contamination or loss of $^{26}Mg^*$ requires a perfect offset with the $^{27}Al^+$ signal, which is unlikely. Zinner & Jadhav (2013) detail a couple of examples where the assumption of constant Al contamination does not hold (see Figures 4–5 of Zinner & Jadhav 2013), showing s-shaped correlation plots. One such example in the current work is from the SiC grain LS-6 (Zinner & Jadhav unpublished; Figure 11). The depth profile was split between regimes where the ion signals were increasing at different rates and where each signal had generally reached equilibrium. The effect of the changing ion signals is apparent in the isochron plot (Figure 11(b)). In the inset, marker faces were shaded by increasing measurement time with light shading indicating early times and darker shading for later times. During the first 100 s there was a spurious correlation between the $\delta^{26}Mg/^{24}Mg$ and $^{27}Al/^{24}Mg$ ratios; between 100 and 450 s the correlation disappeared, although the $\delta^{26}Mg/^{24}Mg$ values continued to rise throughout the profile. This s-shaped correlation plot was likely due to the presence of small grains on the surface of LS-6 containing smaller quantities of $^{26}Mg^*$ or was due to insufficient presputtering time. For example, isotopic imaging revealed small Si-rich contaminant grains, whose Si isotope ratios match those of Mainstream SiC grains, on the surface of the large SiC X-grain "Bonanza" LU-13 (Zinner et al. 2011). Prior measurements of LS-6 with the Cs^+ primary beam also implanted Cs in the grain causing positive secondary ion formation from the O^- primary beam to be suppressed early in the measurement. In addition, implantation of O increases positive ion yields. The Al, Mg, and Si ion signals rose at different rates due to their different ionization energies (Figure 11(a)), which can lead to spurious Al–Mg correlations. For example, Si has a lower ionization efficiency than Al and Al reaches a saturation value much earlier than Si. In this case, using the entire depth profile to make a $^{27}Al/^{24}Mg$ ratio inference yields an incorrect value. A linear ODR fit to the points from 450–750 s in the depth profile, after the ion signals have generally equilibrated, yields a slope of 216 ± 14 ($^{26}Al/^{27}Al = 3.0 \times 10^{-2} \pm 1.8 \times 10^{-3}$) with a $\delta^{26}Mg/^{24}Mg$ intercept of $-11,214 \pm 1716$. In this case the selection of regression points greatly affects the resulting isochron slope. However, note that once the depth profiles reached an equilibrium after 450 s, the resulting isochron fit still negatively intercepts the $\delta^{26}Mg/^{24}Mg$ axis due to Al contamination that was mixed down into the grain during ion probe measurements.

Presputtering until full ion signal equilibration can be detrimental to the analysis of small, submicron presolar grains due to the miniscule amount of material available for measurement. However, since we have observed that the rates of ionization differ for Al and Mg prior to equilibration, the entirety of the depth profiles cannot be used to correctly infer initial $^{27}Al/^{24}Mg$ ratios from either the conventional whole-grain or isochron-fitting method. In this study, care was taken to avoid fitting isochrons to data from unequilibrated depth profiles in an attempt to avoid introducing spurious correlations. Numerous depth profiles from presolar SiC grains also exhibited declining $^{24}Mg^+$ ion signals over the course of the measurement, an indication of decreasing Mg contamination on the grains. For these profiles we also examined the correlation

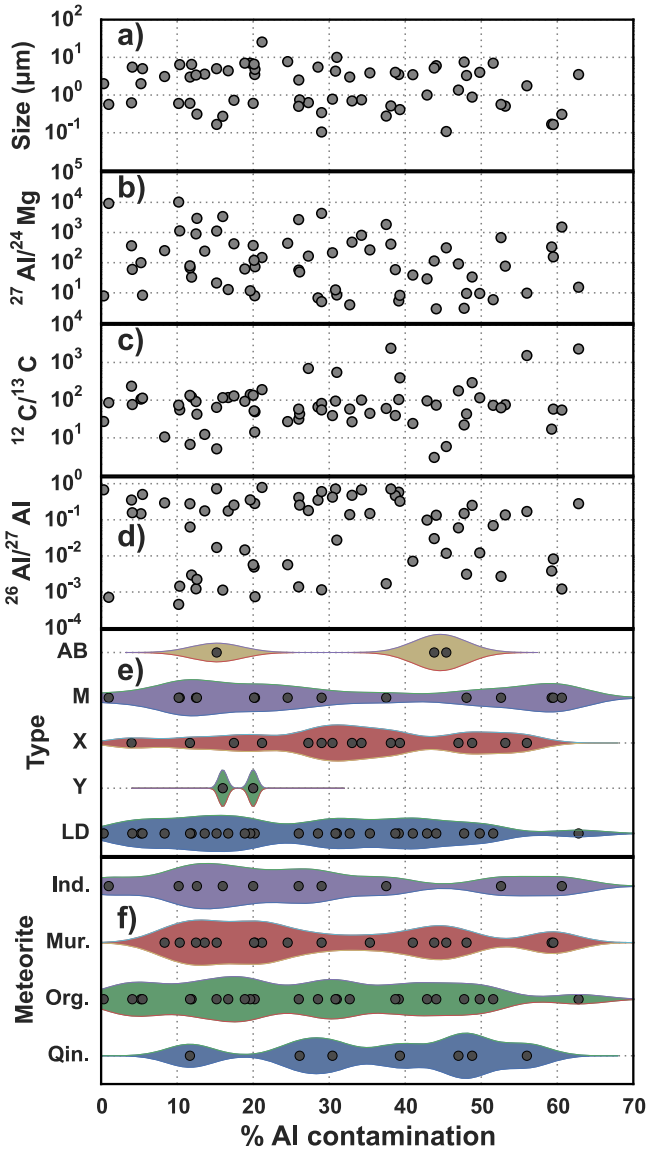

Figure 10. Quantity of fractional Al contamination on each presolar grain is random and independent of other grains. There are no correlations between Al contamination and grain size, ^{27}Al/^{24}Mg ratio, ^{12}C/^{13}C ratio, ^{26}Al/^{27}Al ratio, grain type, or host meteorite. Meteorite abbreviations: Indarch (Ind.); Murchison (Mur.); Orgueil (Org.); Qingzhen (Qin.).

between ^{26}Mg and ^{27}Al to confirm that the isochrons did not result solely from changing ^{24}Mg^{+}. These examples were not the norm for the majority of presolar grains, however, they further highlight the importance of in-depth inspections of each presolar grain's depth profile for the Mg–Al system prior to estimation of initial ^{27}Al/^{24}Mg ratios.

We also inspected the distribution of the ratio of the two estimates ($R = (^{27}\mathrm{Al}/^{24}\mathrm{Mg})_{\mathrm{isochron}}/(^{27}\mathrm{Al}/^{24}\mathrm{Mg})_{\mathrm{whole}}$; Figure 12), which qualitatively follows an exponential distribution ($A \times e^{-(x-1)/\beta}$), where A is the amplitude and β is the scale parameter. The horizontal shift by a value of 1 results from $R \geqslant 1$ for all isochrons with negative δ^{26}Mg/^{24}Mg intercepts, derived in the next paragraph. The distribution has a scale parameter, β, being equal to 1.2 ± 0.2 or 0.76 ± 0.02 for fits to the exponential distribution (Figure 12(a)) and normalized cumulative exponential distribution ($1 - e^{-(x-1)/\beta}$; Figure 12(b)), respectively. For the exponential distribution fit, the correlation between the A and β parameters is −0.7, yielding larger estimated uncertainties for these parameters. The expectation value (mean) and standard deviation of an exponential distribution located at $x = 0$ is β, so the mean of the distribution in Figure 12 lies between 1.76 and 2.2. This is larger than the regression estimate of 1.46 from Figure 5, which itself is closer to the median of the distribution, $\ln(2) \times \beta$. Based upon the linear regression and the distribution of R values, the isochron-derived ^{26}Al/^{27}Al ratios are larger than the whole-grain estimates by a factor of ∼1.5–2, on average.

From the schematic diagram in Figure 7 we derived the relationship between the isochron and mean-value slopes. Letting (X_m, Y_m) be the mean (^{27}Al/^{24}Mg, δ^{26}Mg/^{24}Mg) values of the grain, where X_{i} and X_{c} are the intrinsic and contaminant ^{27}Al/^{24}Mg components, respectively, therefore $X_m = X_{\mathrm{i}} + X_{\mathrm{c}}$. The mean or whole-grain slope is Y_m/X_m whereas the isochron slope is Y_m/X_{i}. Therefore,

$$R_{\mathrm{g}} = \frac{X_{m,\mathrm{g}}}{X_{\mathrm{i,g}}} = \frac{X_{\mathrm{c,g}}}{X_{\mathrm{i,g}}} + 1 \tag{6}$$

where R_{g}, the ratio of mean to intrinsic ^{27}Al/^{24}Mg ratios for each individual grain, g, is linearly dependent upon X_{c} and is always $\geqslant 1$, which is apparent in Figure 12. Substituting the fractional Al contamination, $C = X_{\mathrm{c}}/X_m$ yields:

$$R_{\mathrm{g}} = \frac{X_{m,\mathrm{g}}}{X_{\mathrm{i,g}}} \tag{7a}$$

$$= \frac{X_{m,\mathrm{g}}}{X_{m,\mathrm{g}} - X_{\mathrm{c,g}}} \tag{7b}$$

$$= \frac{1}{1 - C_{\mathrm{g}}}. \tag{7c}$$

Figure 13(a) shows the relationship between C, the fractional Al contamination, and R, the ratio of mean and intrinsic ^{27}Al/^{24}Mg ratios, where the expression derived in Equation (7c) is an excellent match to the lower envelope of the R values. Many R values lie well above the derived line, however, which is partly due to the whole-grain estimates utilizing the entirety of each grain's depth profile and thus sampling sensitivity-biased isotope ratios. Subtracting the derived $1/(1 - C_{\mathrm{g}})$ from each grain's measured R_{g} value yields the distribution shown in Figure 13(b) and its cumulative probability distribution shown in Figure 13(c). Since these distributions contain some negative values, we fitted the distribution to a versatile asymmetric Lorentzian profile:

$$L_{\mathrm{asym.}} = \frac{A}{\pi} \times \frac{w_0 \Big/ \left(1 + e^{a(x-x_0)}\right)}{(x - x_0)^2 + \left(w_0 \Big/ \left(1 + e^{a(x-x_0)}\right)\right)^2} \tag{8a}$$

$$= \frac{A}{\pi} \times \frac{w_0 \left(1 + e^{a(x-x_0)}\right)}{\left(1 + e^{a(x-x_0)}\right)^2 (x - x_0)^2 + w_0^2} \tag{8b}$$

(Stancik & Brauns 2008; Groopman et al. 2014), where the scale parameter, w, was allowed to vary as a sigmoid with x: $w(x) = 2w_0 \Big/ \left(1 + \exp(a(x - x_0))\right)$. This function asymptotically approaches an exponential for $x > x_0$ ($a < 0$ for

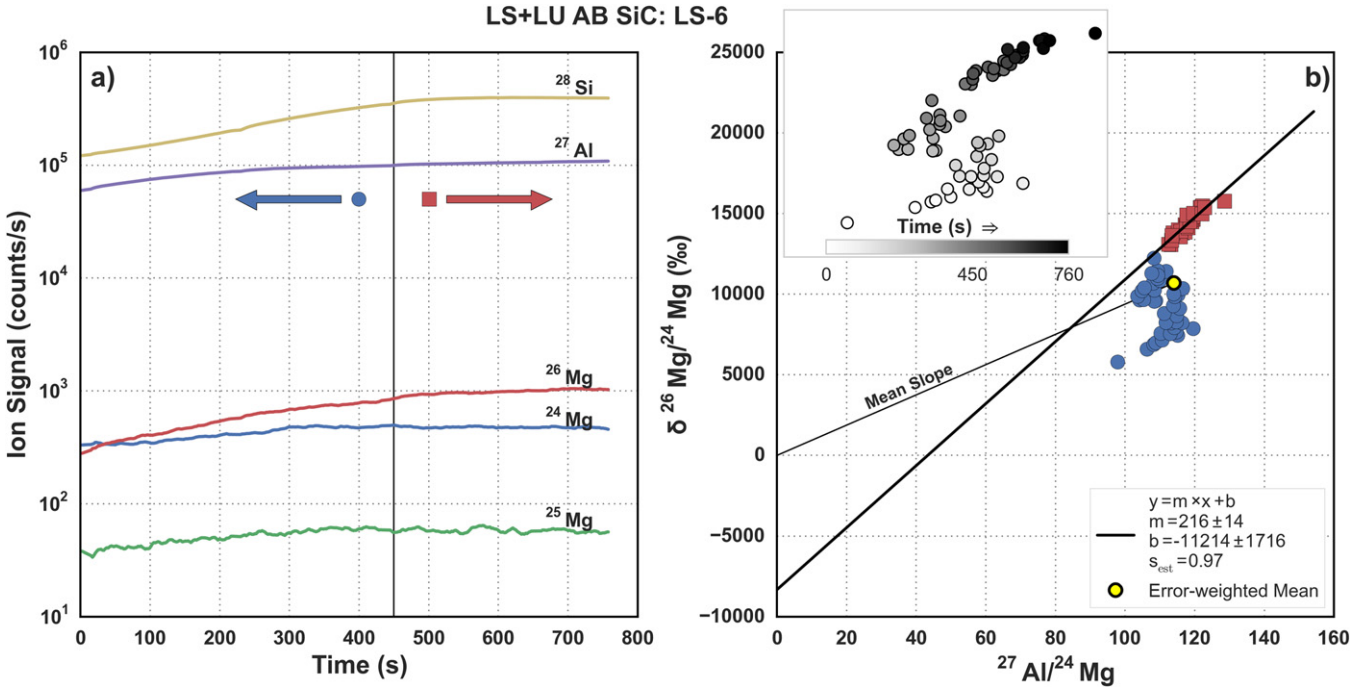

Figure 11. (a) Depth profile of presolar AB SiC grain LS-6 (Zinner & Jadhav, unpublished). During the first 450 s of the profile the Mg, Al, and Si ion signals are increasing at different rates yielding spurious correlations in panel (b). After 450 s the ion signals equilibrate, as does the correlation line. Inset shows each bin shaded by measurement time. After equilibration, the isochron $\delta^{26}Mg/^{24}Mg$ intercept remains negative, indicating that there remains Al contamination throughout the depth profile. The isochron slope also remains steeper than the mean slope from the whole profile.

positively skewed distributions; skew = 1.9) and its good fit to the data further indicates that the underlying distribution of R values is exponential. The cumulative probability distribution for a Cauchy (Lorentzian) distribution is an arctangent, so we easily derived the asymmetric version using the same scale parameter substitution:

$$\frac{1}{2} + \frac{1}{\pi} \times \tan^{-1}\left(\left(x - x_0\right)\left(1 + e^{a(x-x_0)}\right)\Big/\left(2w_0\right)\right). \quad (9)$$

Exponential distributions typically describe events that occur continuously and independently at an average constant rate, such as the time interval between successive random events (Bulmer 1979). The R distribution (Figures 12, 13) represents the differences between the two estimates of each grain's initial $^{26}Al/^{27}Al$ ratio, which not only incorporates influences from Al contamination, which is uniformly random, but also again emphasizes the need to critically investigate each presolar grain's depth profile prior to inferring the presence of extinct radionuclides in order to avoid large systematic errors in their derived initial compositions.

Al contamination, assumed constant through these depth profiles, is clearly present on presolar grains' surfaces. For the smallest SiC grains, it is possible that Al impurities in the Au foil substrates on which the grains were deposited for SIMS analysis (typically >5N purity) contributed to the $^{27}Al^+$ signals, as NanoSIMS raster sizes were typically larger than the grains. However, we postulate that the grains, whose surfaces were etched during the meteorite acid separation (Bernatowicz et al. 2003) trapped dissolved Al contamination from the meteorite in their etched surface grooves. Additionally, small Al-rich crystals adhered to the surfaces of presolar graphite grains have been observed with the TEM. SIMS presputtering and subsequent measurements resulted in mixing some of this contamination deeper into the grains. Given the relatively short timescale of these NanoSIMS measurements, the Al contamination might appear relatively constant across the depth profiles. One way to test this hypothesis would be to isolate and measure pristine SiC (Bernatowicz et al. 2003) and graphite grains, whose surfaces are not chemically etched and which never came into contact with dissolved Al-bearing minerals. Since SN grains have the largest $^{26}Al/^{27}Al$ ratios, these grains would be the most diagnostic. SiC X grains typically account for only 1% of all presolar SiC grains, so a large number of pristine grains would be required to locate a large enough sample for meaningful statistics. However, due to the relatively low Mg abundances in presolar SiC grains (e.g., Hoppe et al. 1994, Figure 14), when a characteristic Mg energy dispersive X-ray spectrum (EDXS) is detectable in the scanning electron microscope (SEM) it is often due exclusively to the presence of radiogenic ^{26}Mg so this may be used to rapidly locate X grains prior to NanoSIMS analyses (F. Gyngard & M. Hynes, 2015 private communication). Pristine LD graphite grains could be isolated and concentrated via centrifugation in the density range ($1.6 < \rho < 2.0$ g cm^{-3}). Since presolar graphite grains are often quasi-spherical with distinct surface morphologies, correlated EDXS, secondary electron imaging, and image processing techniques could be used to automatically identify dispersed graphite grains on Au foil substrates in the SEM.

3.3. Al-rich Presolar Oxide Grains

We processed the depth profiles of 14 presolar hibonite grains from the Krymka unequilibrated ordinary chondrite (LL3.1) and one from a mixed residue of the primitive Antarctic chondrites QUE 97008, WSG 95300, and MET 00452 labeled "UOC" (Nittler et al. 2008). Presolar oxide grains were identified by

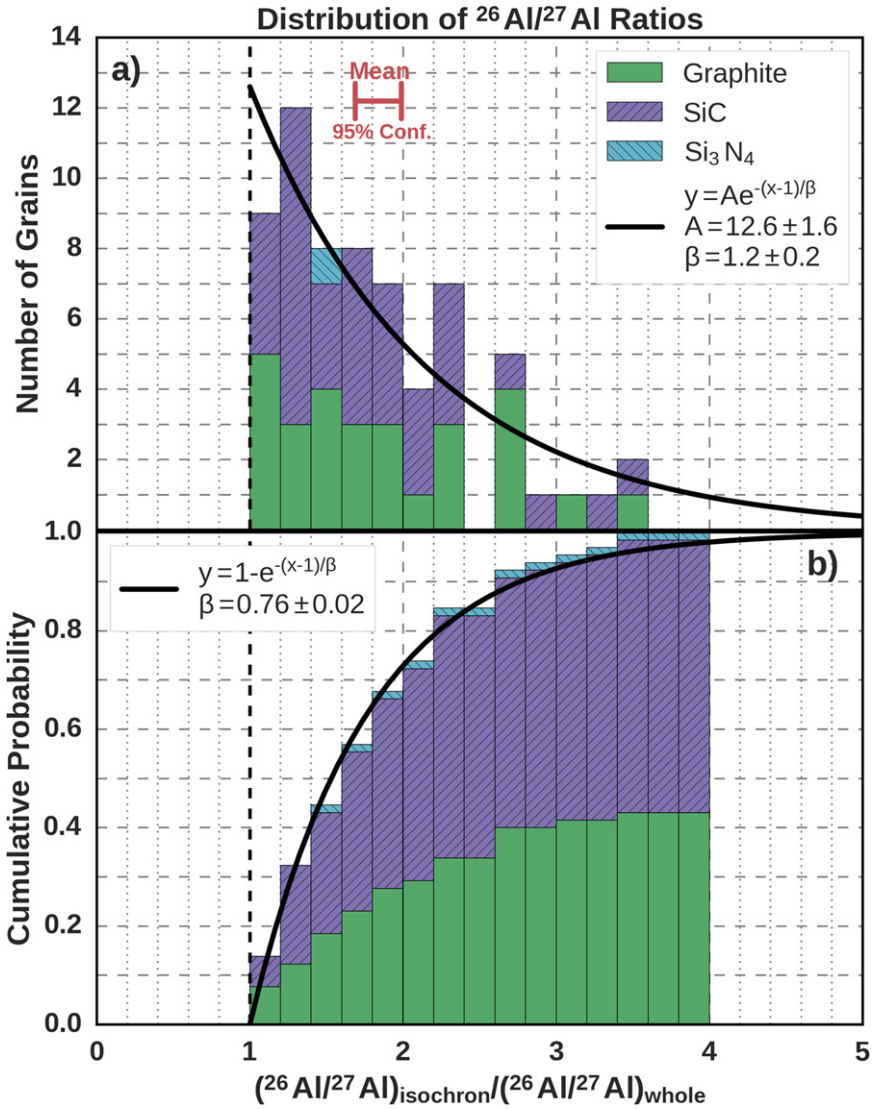

Figure 12. (a) Distribution of ^{26}Al/^{27}Al ratios derived from isochron slopes relative to the ^{26}Al/^{27}Al ratios derived from whole-grain estimates for grains with negative δ^{26}Mg/^{24}Mg intercepts. (b) Normalized cumulative distribution with fit to a cumulative exponential distribution. The exponential distributions are shifted by a value of 1 to the right. The expectation value of an exponential distribution is equal to β plus the shift in x. Based upon the two fits, the mean value of the distribution lies between 1.76 ± 0.02 and 2.2 ± 0.2, which matches the bootstrapped 95% confidence interval shown in panel (a). We are therefore confident that the distribution can be well modeled by an exponential.

automated isotopic measurements with the Cameca IMS 6f ion probe at the Carnegie Institution of Washington and later measured with the Washington University NanoSIMS 50, or, for the UOC grain, the Carnegie NanoSIMS 50(L). Twelve of the 14 Krymka grains contained appreciable ^{26}Mg* with ^{26}Al/^{27}Al ratios ranging between 6.2×10^{-5} and 1.2×10^{-1} from whole-grain measurements. However, the $^{27}Al^+$ and $^{24}Mg^+$ ion signals hardly fluctuated across the short depth profiles, resulting in minimal spread in the ^{27}Al/^{24}Mg ratios. We could therefore not fit any isochron lines to these data. The presolar hibonite grain UOC-H2 does exhibit a fairly well defined isochron line (Figure 15), however, with a positive δ^{26}Mg/^{24}Mg intercept we cannot glean any information regarding the effect of Al contamination. Since Al is a major element in hibonite and its ion signal does not vary through the depth profiles, evidence for the loss of ^{26}Mg* should be apparent, if present. The $^{26}Mg^+$ ion signals would be expected to vary uncorrelated to the $^{27}Al^+$ ion signals. As we observe little variation through all of the ion signals, we may discount the possibility of ^{26}Mg* loss. The Al and Mg ion signals from presolar SiC and graphite grains cannot be a priori assumed to be constant across the depth profiles as both elements are minor or trace constituents of the bulk grains and could be heterogeneously distributed within. Hibonite is not a perfect analog to presolar graphite and SiC grains, however, as radiogenic ^{26}Mg atoms in hibonite grains would occupy the same crystal lattice sites as their radioactive ^{26}Al parent atoms, and would therefore presumably be more tightly bound within the crystal than in graphite or SiC. The question naturally left open is the full extent of matrix effects from the different mineral types on processes such as contamination and radiogenic isotope loss; however this lies beyond the scope of this paper.

3.4. Supernova Models

Prior to exploding as Type II SNe, massive stars have an onion-like structure, with the compositions of different shells reflecting the differing degrees of nuclear burning the material

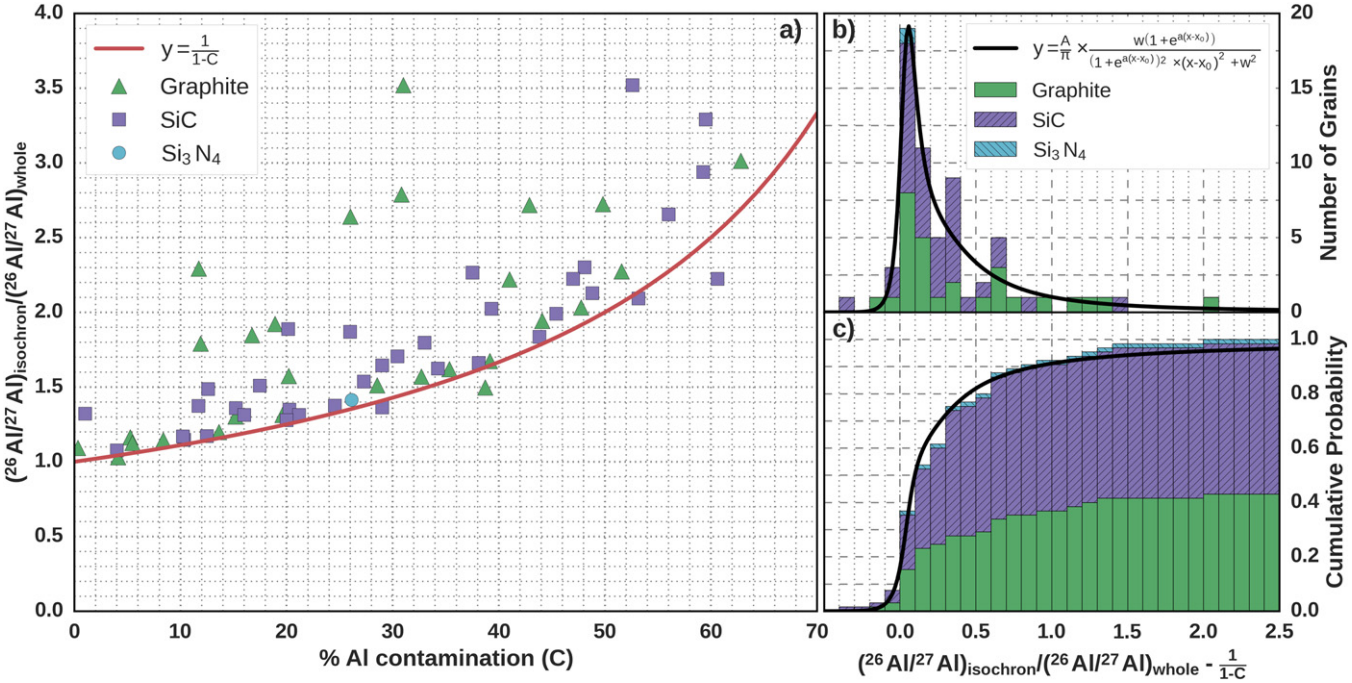

Figure 13. (a) Relationship between R, the relative ratio of $^{26}Al/^{27}Al$ inferred from each grain's isochron slope and whole-grain measurement, and fractional Al contamination. The geometrically derived relationship (shown in red online) matches well the envelope of R values. Values higher than this line are due in large part to inferring isotope ratios from ion signals prior to equilibration in whole-grain estimates. (b) Distribution of R values after subtraction of geometric relationship, well-fitted by an asymmetric Lorentzian profile, which above the median value, x_0, is approximately exponential ($a < 0$). (c) Cumulative distribution with fit to cumulative asymmetric Lorentzian profile.

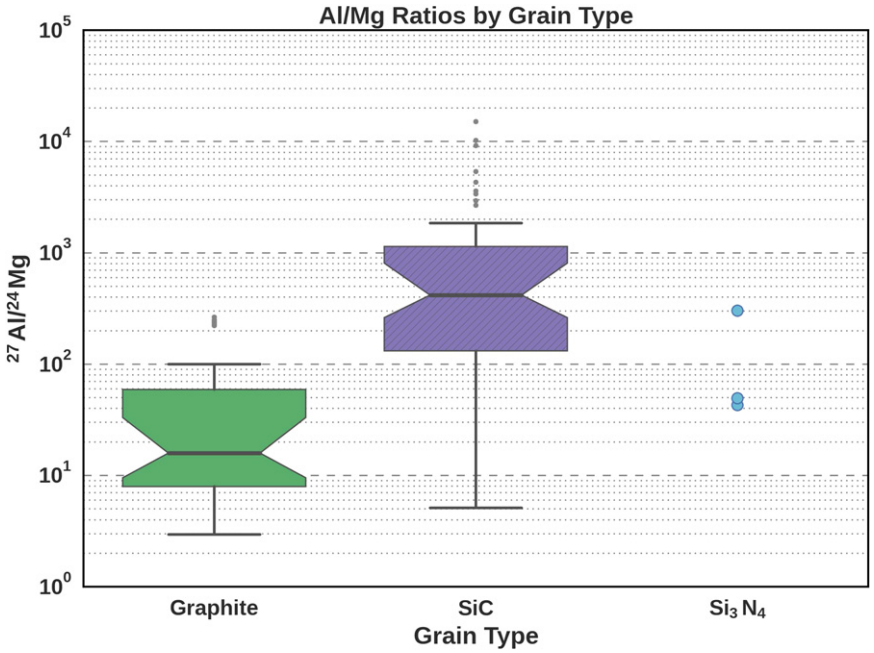

Figure 14. Comparison of Al/Mg ratios in presolar graphite and SiC grains. Only a small factor in the difference between graphite and SiC grains could be a matrix effect, i.e., different relative sensitivity factors. Filled regions of the box plots show the interquartile range (IQR; 25%–75%), with a median line; whiskers extend to 1.5 × IQR past the closest quartile. Bootstrapped 95% confidence intervals on the median lines are shown by notches in the boxplots.

has experienced during the pre-SN evolution. Recent isotopic, microstructural, and theoretical studies (Groopman et al. 2012, 2014; Jadhav et al. 2013; Pignatari et al. 2013; Amari et al. 2014) have concluded that the He/C and He/N SN zones (named for the most abundant chemical species, Meyer et al. 1995) are the most likely dominant sources of material that condensed to form presolar SN graphite and SiC grains, with small contributions from the much deeper Si/S zone. The He/N zone, which has experienced complete H burning, was previously assumed to be the source of high inferred initial $^{26}Al/^{27}Al$ ratios in SN grains. However, 16 of the 90 presolar grains in the current study have initial $^{26}Al/^{27}Al$ ratios inferred

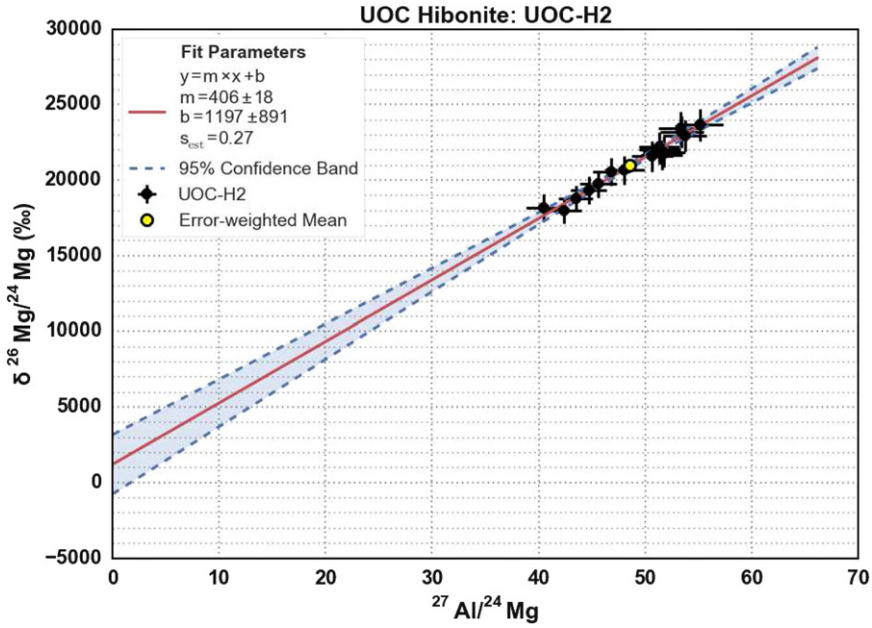

Figure 15. Al–Mg isochron of presolar hibonite UOC-H2 (Nittler et al. 2008). $^{26}Al/^{27}Al = 5.9 \times 10^{-2} \pm 3 \times 10^{-3}$.

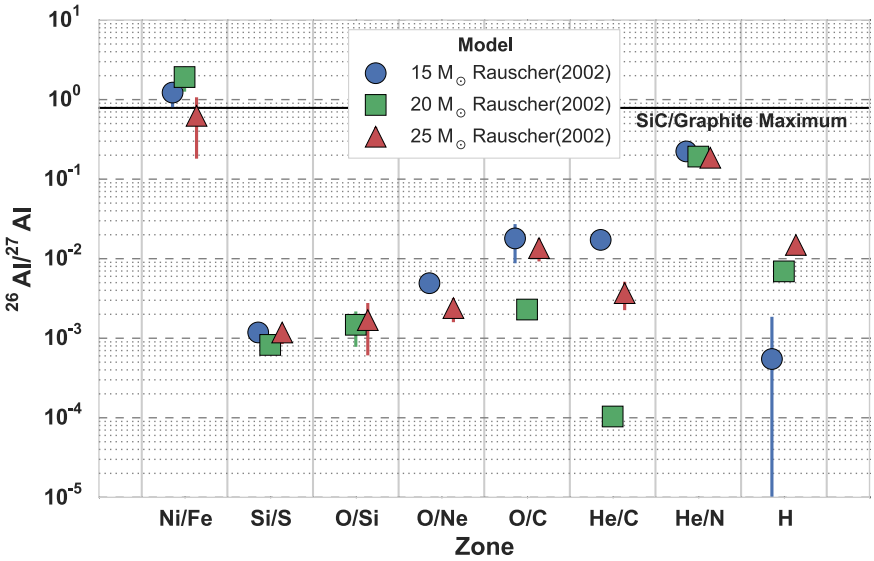

Figure 16. Comparison of SN models from Rauscher et al. (2002) showing the mass-weighted mean $^{26}Al/^{27}Al$ ratios within the major SN zones. Only the Fe/Ni zone in some models can reproduce upper range of $^{26}Al/^{27}Al$ ratios in presolar grains. Error bars show the standard deviation of the $^{26}Al/^{27}Al$ ratio across each zone. Solid horizontal line indicates the largest $^{26}Al/^{27}Al$ ratios from presolar SiC and graphite grain isochrons.

from their isochron slopes greater than the maximum $^{26}Al/^{27}Al$ ratios in the He/N ($^{26}Al/^{27}Al < 0.34$) and He/C ($^{26}Al/^{27}Al < 0.16$) zones of SN models with a range of initial masses (Figure 16), confirming the findings of previous studies (e.g., Lin et al. 2010; Jadhav et al. 2013). Only the Ni/Fe zone in these models can reproduce the $^{26}Al/^{27}Al$ ratios in these grains, however, the Al abundance in this zone is low. The contribution of Ni/Fe zone Al is likely to be overwhelmed by Al from the outer zones resulting in low $^{26}Al/^{27}Al$ ratios. Furthermore, any amount of Al from the Ni core would result in large ^{56}Fe excesses in SiC X grains, which are not observed (Marhas et al. 2008). In order to reproduce the presolar grain data, SN models will need to predict higher $^{26}Al/^{27}Al$ ratios from the He/C and He/N zones and have higher ^{26}Al yield accuracy (Rauscher et al. 2002). Improved SN yields of ^{26}Al are additionally of great importance to models of the early SS (Huss et al. 2009).

3.5. K–Ca and Ti–Ca Isochrons

The widespread application of isochron analysis discussed here to the Ca–K and Ti–Ca systems is complicated by a number of factors. Potassium is a volatile element and a widespread contaminant on sample mounts. The Ca–K sensitivity factor derived from Ca and K elemental abundances is therefore highly sensitive to each sample's and standard's surface morphology. Potassium is such a widespread contaminant that, for many of the published Ca–K data (e.g., Jadhav et al. 2013), stoichiometric standards with both K and

Ca were not used, rather the NanoSIMS $^{41}K/^{39}K$ ratios were normalized based upon the contamination signal alone, assuming a normal isotopic composition. Accurate Ca–K relative sensitivity factors cannot be obtained in these cases. Moreover, compared to presolar grains with evidence for radiogenic $^{26}Mg^*$, there are many fewer grains with evidence for radiogenic $^{41}K^*$, limiting a statistical study.

The majority of Ti within SN graphite grains is concentrated in Ti-rich subgrains, most often TiC. During each primary beam raster scan of a grain's surface, the NanoSIMS may be sampling any number of distinct Ti-rich subgrains, greatly confounding an isochron fit. Additionally, Zinner & Jadhav (2013) found that in graphite grains the bulk of the Ca ion signals originated from within the graphite structure and not from the TiC subgrains, where radiogenic ^{44}Ca resides. This results in spatially varying Ti–Ca relative sensitivity factors between the graphite host grain and its TiC subgrains. These intricacies cannot be properly dealt with via one-dimensional depth profiling and would require image-mode depth profiling. Given the high time cost of acquiring isotope image depth profiles, these data are not available for the vast majority of grains.

4. CONCLUSIONS

A reanalysis of SIMS Al–Mg depth profiles of 450 previously reported presolar grains reveals that a majority of the measurements included significant contamination in their measured Al signals, often making it impossible to infer the initial $^{26}Mg/^{24}Mg$ ratio of the sample. For presolar grains whose isochrons positively intercept the $\delta^{26}Mg/^{24}Mg$ axis, whole-grain $^{26}Al/^{27}Al$ ratio calculations overestimate the true initial ratio. The majority of isochrons, however, have negative $\delta^{26}Mg/^{24}Mg$ intercepts, often with an unphysical value lower than −1000‰. The analysis of 15 hibonite grains, 13 of which contained evidence for radiogenic ^{26}Mg, illustrated that $^{26}Mg^*$ was not lost during the grains' lifetimes and that Al contamination is the cause of the negative isochron intercepts for SiC and graphite grains. The amount of Al contamination may be estimated as the shift required for the isochron to intercept the origin. The distribution of fractional Al contamination was found to be uniform for both presolar SiC and graphite grains up to ∼59%, implying that the quantity of contamination of each grain is random and independent of other grains. The uniform Al contamination distribution is modulated (stretched to larger values) by the presence of Mg contamination. The conventional whole-grain method for inferring initial $^{26}Al/^{27}Al$ ratios, by essentially calculating the slope of the line between the average $\delta^{26}Mg/^{24}Mg$ and $^{27}Al/^{24}Mg$ values and the origin, underestimates the isochron-derived $^{26}Al/^{27}Al$ ratios by a factor of ∼1.5–2 on average. Many presolar grains from SNe have $^{26}Al/^{27}Al$ ratios that far exceed the ratios predicted for the He/C and He/N zones, the most likely source of the grains in models of core-collapse SNe. It remains to be determined whether higher ^{26}Al yields in SN models may explain the presolar grain data.

The authors thank the referee for a careful review of this paper and Thomas Bernatowicz for helpful discussions. This work was funded, in part, by NASA grants NNX10AI45G (TB), NNX11AH14G (EZ), and NNX10AI63G (LN).

REFERENCES

Alpher, R. A., & Herman, R. C. 1950, RvMP, 22, 153
Amari, S. 2009, ApJ, 690, 1424
Amari, S., Anders, E., Virag, A., & Zinner, E. 1990, Natur, 345, 238
Amari, S., Lewis, R. S., & Anders, E. 1994, GeCoA, 58, 459
Amari, S., Nittler, L. R., Zinner, E., Lodders, K., & Lewis, R. S. 2001a, ApJ, 559, 463
Amari, S., Nittler, L. R., Zinner, E., et al. 2001b, ApJ, 546, 248
Amari, S., Zinner, E., & Gallino, R. 2014, GeCoA, 133, 479
Amari, S., Zinner, E., & Lewis, R. S. 1996, ApJL, 470, L101
Bernatowicz, T. J., Amari, S., Zinner, E., & Lewis, R. S. 1991, ApJL, 373, L73
Bernatowicz, T. J., Fraundorf, G., Tang, M., et al. 1987, Natur, 330, 728
Bernatowicz, T. J., Messenger, S., Pravdivtseva, O., Swan, P., & Walker, R. M. 2003, GeCoA, 67, 4679
Black, D. C., & Pepin, R. O. 1969, E&PSL, 6, 395
Boggs, P. T., & Rogers, J. E. 1990, in Contemporary Mathematics: Statistical Analysis of Measurement Error Models and Applications, Vol. 112, ed. P. J. Brown & W. A. Fuller (Providence, RI: American Mathematical Society), 1
Boggs, S. E., Harrison, F. A., Miyasaka, H., et al. 2015, Sci, 348, 670
Bulmer, M. G. 1979, Principles of Statistics (New York: Dover)
Burbidge, E. M., Burbidge, G. R., Fowler, W. A., & Hoyle, F. 1957, RvMP, 29, 547
Cameron, A. G. W. 1957, PASP, 69, 201
Choi, B. G., Wasserburg, G. J., & Huss, G. R. 1999, ApJL, 522, L133
Davis, A. M., & McKeegan, K. 2014, in Treatise on Geochemistry, ed. H. D. Holland & H. K. Turekian (2nd ed.; Oxford: Elsevier), 36
Diehl, R. 2011, in Astronomy with Radioactivities, Vol. 812, ed. R. Diehl, D. H. Hartmann & N. Prantzos (Berlin: Springer), 3
Diehl, R. 2014, in AIP Conf. Proc. 1594, Origin of Matter and Evolution of Galaxies 2013, ed. S. Jeong et al. (New York: AIP), 109
Diehl, R., Bennett, K., Bloemen, H., et al. 1993, A&AS, 97, 181
Diehl, R., Halloin, H., Kretschmer, K., et al. 2006, Natur, 439, 45
Diehl, R., Hartmann, D. H., & Prantzos, N. 2007, M&PS, 42, 1145
Diehl, R., Siegert, T., Hillebrandt, W., et al. 2015, A&A, 574, A72
Fujiya, W., Hoppe, P., Zinner, E., Pignatari, M., & Herwig, F. 2013, ApJL, 776, L29
Grefenstette, B. W., Harrison, F. A., Boggs, S. E., et al. 2014, Natur, 506, 339
Groopman, E., Bernatowicz, T., & Zinner, E. 2012, ApJL, 754, L8
Groopman, E., Nittler, L. R., Bernatowicz, T., & Zinner, E. 2014, ApJ, 790, 9
Herwig, F., Pignatari, M., Woodward, P. R., et al. 2011, ApJ, 727, 89
Hoppe, P., Amari, S., Zinner, E., Ireland, T., & Lewis, R. S. 1994, ApJ, 430, 870
Hoppe, P., Amari, S., Zinner, E., & Lewis, R. S. 1995, GeCoA, 59, 4029
Hoppe, P., Annen, P., Strebel, R., et al. 1997, ApJL, 487, L101
Hoppe, P., & Besmehn, A. 2002, ApJL, 576, L69
Hoppe, P., Leitner, J., Gröner, E., et al. 2010, ApJ, 719, 1370
Hoyle, F. 1946, MNRAS, 106, 343
Hoyle, F. 1954, ApJS, 1, 121
Huss, G. R., Meyer, B. S., Srinivasan, G., Goswami, J. N., & Sahijpal, S. 2009, GeCoA, 73, 4922
Hutcheon, I. D., Huss, G. R., Fahey, A. J., & Wasserburg, G. J. 1994, ApJL, 425, L97
Hynes, K. M., & Gyngard, F. 2009, LPSC Vol. 40 (Houston: Lunar and Planetary Institute)
Jacobsen, B., Yin, Q., Moynier, F., et al. 2008, E&PSL, 272, 353
Jadhav, M., Amari, S., Zinner, E., & Maruoka, T. 2006, NewAR, 50, 591
Jadhav, M., Zinner, E., Amari, S., et al. 2013, GeCoA, 113, 193
Kashiv, Y., Davis, A. M., Gallino, R., et al. 2010, ApJ, 713, 212
Lee, T., Panastassiou, D. A., & Wasserburg, G. J. 1976, GeoRL, 3, 109
Leibundgut, B., & Suntzeff, N. 2003, in Supernovae and Gamma-Ray Bursters, Vol. 598, ed. K. W. Weiler (Berlin: Springer), 77
Leising, M. D., & Share, G. H. 1990, ApJ, 357, 638
Lewis, R. S., Ming, T., Wacker, J. F., Anders, E., & Steel, E. 1987, Natur, 326, 160
Lin, Y., Amari, S., & Pravdivtseva, O. 2002, ApJ, 575, 257
Lin, Y., Gyngard, F., & Zinner, E. 2010, ApJ, 709, 1157
Marhas, K. K., Amari, S., Gyngard, F., Zinner, E., & Gallino, R. 2008, ApJ, 689, 622
Matz, S. M., Share, G. H., Leising, M. D., et al. 1988, Natur, 331, 416
McSween, H. Y., Jr., & Hus, G. R. 2010, Cosmochemistry (Cambridge: Cambridge Univ. Press)
Merrill, P. W. 1952, ApJ, 116, 21
Messenger, S., Keller, L. P., Stadermann, F. J., Walker, R. M., & Zinner, E. 2003, Sci, 300, 105

Meyer, B. S., Weaver, T. A., & Woosley, S. E. 1995, Metic, 30, 325
Meyer, B. S., & Zinner, E. 2006, In Meteorites and the Early Solar System II (Tuscon, AZ: Univ. Arizona Press)
Nguyen, A. N., & Zinner, E. 2004, Sci, 303, 1496
Nittler, L. R., Alexander, C. M. O'D., Gallino, R., et al. 2008, ApJ, 682, 1450
Nittler, L. R., Alexander, C. M. O'D., Gao, X., Walker, R. M., & Zinner, E. 1997, ApJ, 483, 475
Nittler, L. R., Alexander, C. M. O'D., Gao, X., Walker, R. M., & Zinner, E. K. 1994, Natur, 370, 443
Nittler, L. R., Amari, S., Zinner, E., Woosley, S. E., & Lewis, R. S. 1996, ApJL, 462, L31
Nittler, L. R., Hoppe, P., Alexander, C. M. O'D., et al. 1995, ApJL, 453, L25
Pignatari, M., Zinner, E., Bertolli, M. G., et al. 2013, ApJL, 771, L7
Rauscher, T., Heger, A., Hoffman, R. D., & Woosley, S. E. 2002, ApJ, 576, 323
Renaud, M., Vink, J., Decourchelle, A., et al. 2006, ApJL, 647, L41
Reynolds, J. H., & Turner, G. 1964, JGR, 69, 3263
Savina, M. R., Davis, A. M., Tripa, C. E., et al. 2004, Sci, 303, 649
Stancik, A. L., & Brauns, E. B. 2008, Vib. Spectrosc., 47, 66
Tang, M., & Anders, E. 1988, GeCoA, 52, 1235
Vink, J., Laming, J. M., Kaastra, J. S., et al. 2001, ApJL, 560, L79
Wang, W., Harris, M. J., Diehl, R., et al. 2007, A&A, 469, 1005
Xu, Y., Zinner, E., Gallino, R., et al. 2015, ApJ, 799, 156
Xu, Y. C., Amari, S., Gyngard, F., Zinner, E., & Lin, Y. 2012, LPSC Vol. 43 (Houston: Lunar and Planetary Institute)
Zinner, E. 2014, in Treatise on Geochemistry, ed. K. K. Turekian & H. D. Holland (2nd ed.; Oxford: Elsevier), 181
Zinner, E., Amari, S., Anders, E., & Lewis, R. 1991, Natur, 349, 51
Zinner, E., Amari, S., Guinness, R., et al. 2007, GeCoA, 71, 4786
Zinner, E., & Jadhav, M. 2013, ApJ, 768, 100
Zinner, E., Jadhav, M., Gyngard, F., & Nittler, L. R. 2011, in LPSC Vol. 42 (Houston: Lunar and Planetary Institute), 1070
Zinner, E., Nittler, L. R., Hoppe, P., et al. 2005, GeCoA, 69, 4149